LETTERS

Arc-parallel flow in the mantle wedge beneath Costa Rica and Nicaragua

Kaj Hoernle[1,2], David L. Abt[3], Karen M. Fischer[3], Holly Nichols[1], Folkmar Hauff[2], Geoffrey A. Abers[4]†, Paul van den Bogaard[1,2], Ken Heydolph[1], Guillermo Alvarado[5], Marino Protti[6] & Wilfried Strauch[7]

Resolving flow geometry in the mantle wedge is central to understanding the thermal and chemical structure of subduction zones, subducting plate dehydration, and melting that leads to arc volcanism, which can threaten large populations and alter climate through gas and particle emission. Here we show that isotope geochemistry and seismic velocity anisotropy provide strong evidence for trench-parallel flow in the mantle wedge beneath Costa Rica and Nicaragua. This finding contradicts classical models, which predict trench-normal flow owing to the overlying wedge mantle being dragged downwards by the subducting plate. The isotopic signature of central Costa Rican volcanic rocks is not consistent with its derivation from the mantle wedge[1–3] or eroded fore-arc complexes[4] but instead from seamounts of the Galapagos hotspot track on the subducting Cocos plate. This isotopic signature decreases continuously from central Costa Rica to northwestern Nicaragua. As the age of the isotopic signature beneath Costa Rica can be constrained and its transport distance is known, minimum northwestward flow rates can be estimated (63–190 mm yr^{-1}) and are comparable to the magnitude of subducting Cocos plate motion (~85 mm yr^{-1}). Trench-parallel flow needs to be taken into account in models evaluating thermal and chemical structure and melt generation in subduction zones.

Preferential alignment of the minerals olivine and orthopyroxene occurs as a result of deformation, and produces anisotropy in seismic-wave velocities within the upper mantle. Assuming classical trench-normal 'corner flow' and standard models of crystallographic fabric development, the direction of fast shear-wave polarization will be normal to the arc in the warmer wedge beneath the arc and back-arc, although the fast shear-wave polarization may be parallel to the arc in the cold corner of the wedge beneath the fore-arc[5,6]. Whereas this pattern of seismic anisotropy is observed in some subduction zones[7,8], many display more variable fast directions further from the trench beneath the arc and back-arc, often with a roughly arc-parallel trend[9–12]. The origin of this arc-parallel fast anisotropy, in particular whether it is related to along-arc flow within the mantle wedge or some other process, is vigorously debated[5,6,13–16].

Although arc volcanic rocks from Costa Rica have ocean-island-basalt (OIB)-type compositions similar to those found in Galapagos hotspot rocks[17], the origin of this geochemical signature is controversial. In some models, OIB signatures are contained in the mantle wedge beneath central Costa Rica, reflecting (1) residual Galapagos-type mantle remaining after the formation of the Caribbean large igneous province (CLIP) in the Cretaceous period[1], or flow of OIB-type asthenospheric mantle either (2) from beneath the northwest margin of South America[2] or (3) through a slab window[3] into the mantle wedge beneath central Costa Rica. Alternatively, subduction erosion of older Galapagos and CLIP terranes in the Costa Rican fore-arc may have introduced this signature beneath Costa Rica[4]. The geochemical evidence presented here, however, suggests that the OIB signature is primarily derived from the subducting Galapagos hotspot track.

Central American volcanism results from subduction of the Cocos plate beneath the Caribbean plate (Fig. 1). Normal oceanic crust formed at the East Pacific Rise (EPR) subducts beneath Guatemala

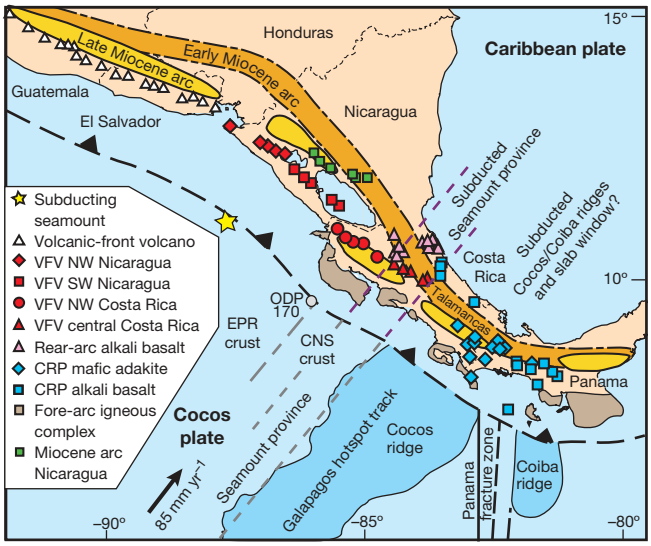

Figure 1 | Reference map of Central America illustrating the subduction of the Galapagos hotspot Seamount province beneath central Costa Rica and the westward migration of the volcanic arc that extends from Costa Rica to southwestern Guatemala. Positions of the arc are shown from the Early Miocene (11–24 Myr ago) to the Late Miocene (6–12 Myr ago) to the Quaternary[30]. The Seamount province of the Galapagos hotspot track is subducting beneath the central Costa Rican volcanic front and Late Pliocene-Holocene (0–2 Myr ago) rear- and back-arc alkali basalts (northeastern occurrences dated at 2 Myr ago). The Cocos and Coiba ridges of the Galapagos hotspot tracks are subducting beneath Pliocene-Holocene mafic adakites and alkali basalts from southeastern Costa Rica and western Panama (CRP), where there has been no volcanic-front volcanism since the Late Miocene. The heavy dashed purple lines project the Seamount province beneath Costa Rica. The boundary between crust formed at the East Pacific Rise (EPR) and the Cocos Nazca (Galapagos) spreading centre (CNS) and the Panama fracture zone are also shown. Volcanic-front volcanoes (VFV) are indicated. A window in the subducting Cocos and Nazca plates may be located beneath southern Costa Rica and western Panama[3].

[1]SFB 574, [2]Leibniz Institute of Marine Sciences (IFM-GEOMAR), University of Kiel, Wischhofstrasse 1-3, Kiel 24148, Germany. [3]Department of Geological Sciences, Brown University, Box 1846, Providence, Rhode Island 02912, USA. [4]Boston University, Department of Earth Sciences, 675 Commonwealth Avenue, Boston, Massachusetts 02215, USA. [5]Observatorio Sismológico y Vulcanológico de Arenal y Miravalles (OSIVAM), Instituto Costarricense de Electricidad (ICE), Apdo. 10032-1000, Costa Rica. [6]Observatorio Vulcanológico y Sismológico de Costa Rica, Universidad Nacional, Apdo. 86-3000, Heredia, Costa Rica. [7]Instituto Nicaragüense de Estudios Territoriales, Apdo. 2110, Managua, Nicaragua. †Present address: Lamont-Doherty Earth Observatory, Columbia University, Palisades, New York 10964, USA.

to northwestern Costa Rica, whereas crust formed at the Cocos-Nazca spreading centre (CNS) with the Galapagos hotspot track on it subducts beneath central Costa Rica to Panama. The Galapagos hotspot tracks (and islands) are chemically zoned[18,19], with the Seamount province having distinctly higher $^{208}Pb/^{204}Pb$ (Figs 1, 2) and lower $^{143}Nd/^{144}Nd$ (Supplementary Fig. 1.1) for a given $^{206}Pb/^{204}Pb$ isotope ratio compared with the Cocos and Coiba ridges.

Radiogenic isotope ratios, which are not fractionated by physical processes such as partial melting and magma differentiation, can be used as tracers to determine the sources contributing to arc magmatism. Along the volcanic front from central Costa Rica to northwestern Nicaragua, Nd isotope ratios increase and Pb isotope ratios decrease continuously (Fig. 2a, b). $^{206}Pb/^{204}Pb$ and $^{208}Pb/^{204}Pb$ isotope data from the volcanic-front rocks also form an excellent linear correlation ($R^2 = 0.997$; Fig. 2c). Although normal arc magmatism ceased in the Late Miocene-Pliocene in southern Costa Rica and western Panama, Pliocene-Quaternary adakitic/alkalic volcanic rocks are widely distributed but volumetrically insignificant[3,20,21]. Lead isotope data from these rocks also form an excellent linear correlation ($R^2 = 0.976$) below, but sub-parallel to, the trend formed by volcanic-front rocks. The highest Pb isotope ratios in the arc rocks occur in the areas situated above the subducting hotspot track, also characterized by radiogenic Pb.

At least three endmembers are required to explain the Pb and Nd isotope data of the Nicaraguan to Panamanian volcanic rocks (see also Supplementary Fig. 1.1). The northwestern Nicaraguan endmember with unradiogenic Pb and radiogenic Nd reflects addition to the depleted mantle wedge of a slab fluid that contains Pb primarily from the subducting crust (as represented by samples from a subducting seamount) (Figs 1, 2). The southern Costa Rica/Panama endmember with radiogenic Pb but intermediate $^{208}Pb/^{204}Pb$ and $^{143}Nd/^{144}Nd$ could be derived from the subducting Cocos/Coiba ridges[3] and/or eroded fore-arc igneous complexes[4], consisting of CLIP basement and accreted early Cenozoic Galapagos seamounts[22–24]. The only source with the appropriate Pb (radiogenic Pb and high $^{208}Pb/^{204}Pb$) and Nd isotopic composition to derive the central Costa Rica endmember is the Seamount province subducting beneath central Costa Rica. Other potential sources for Pb and Nd, such as tectonically eroded Costa Rica fore-arc[4] and input of Galapagos hotspot mantle through a slab window[3] (which would be expected to have a composition similar to the voluminous Cocos/Coiba ridges—representing the primary composition of the Galapagos plume), have isotopic compositions distinct from the Seamount province and thus cannot explain the observed mixing trends.

If the Galapagos seamount slab component has melt-like properties (is a supercritical fluid/hydrous melt), it could readily transport rare-earth elements (for example, La, Nd) and high-field-strength elements (for example, Nb), consistent with the decrease in La/Yb and increase in Ba/La, U/Th and Ba/Th observed in the volcanic-front lavas from central Costa Rica to northwestern Nicaragua[2,25,26] (see Supplementary Information Section 1 for the role of subducted sediments). The transition from a dominantly fluid-like slab component beneath Nicaragua to melt-like slab components in Costa Rica and Panama may be related to the influx of hot mantle through a slab window in the south[3].

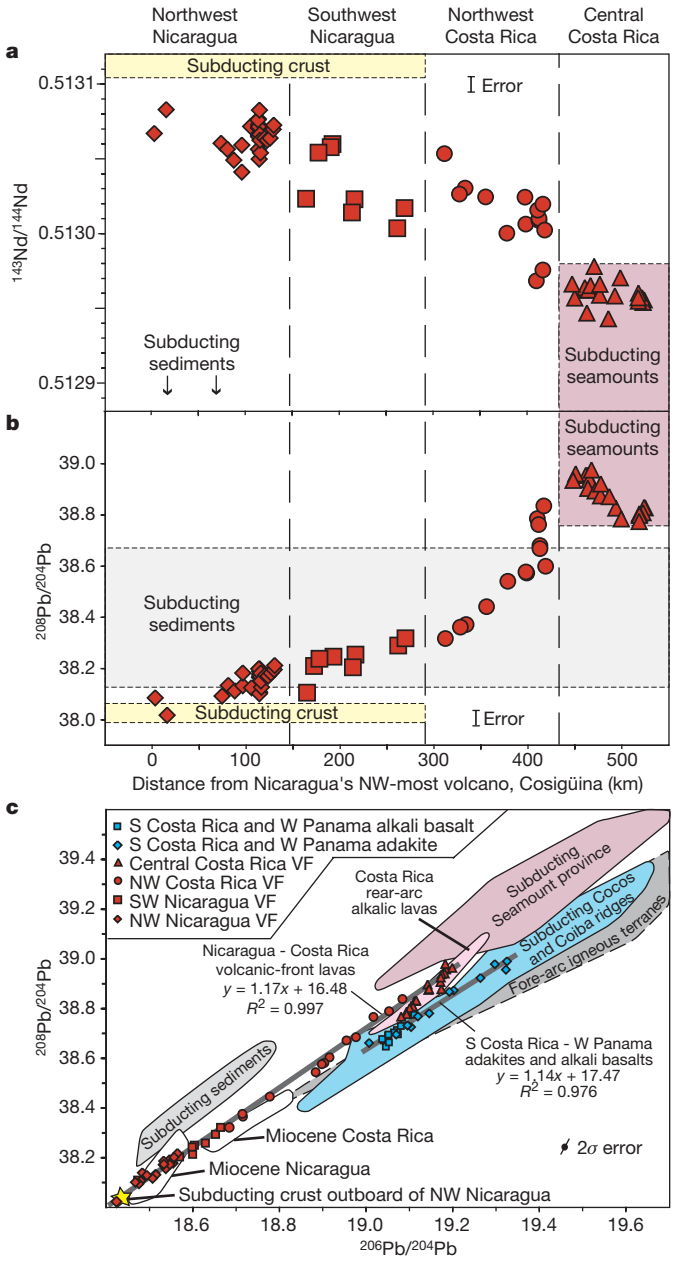

Figure 2 | Systematic variation in lead and neodymium isotopic composition along the volcanic front from Costa Rica to northwest Nicaragua indicates northwestward flow of mantle wedge material. **a**, **b**, Isotope ratios, $^{143}Nd/^{144}Nd$ (**a**) and $^{208}Pb/^{204}Pb$ (**b**), show systematic trends along the arc that indicate mixing of mantle wedge enriched with melts from the subducting Galapagos hotspot Seamount province with mantle wedge enriched with hydrous fluids from the ocean crust subducting beneath Nicaragua. In **c**, Quaternary volcanic front (VF) lavas from Nicaragua and Costa Rica form an excellent linear correlation (longer solid grey line, $R^2 = 0.997$) on the thorogenic Pb isotope diagram. Late Pliocene-Quaternary rear- and back-arc alkalic lavas in northeastern Costa Rica overlap in composition with Costa Rica volcanic-front lavas but extend to more radiogenic compositions, consistent with a greater contribution from a melt-like slab component. Low volume, scattered Pliocene-Quaternary mafic adakites and alkali basalts from southern Costa Rica and western Panama, where there has been no volcanic-front volcanism since the Late Miocene, form a distinct linear array (shorter solid grey line, $R^2 = 0.976$) below but subparallel to the volcanic-front lavas, having lower $^{208}Pb/^{204}Pb$ for a given $^{206}Pb/^{204}Pb$ isotope ratio. Whereas the adakites may represent direct melts of subducted Galapagos rocks, the alkali basalts most probably reflect interaction between carbon-rich fluids/melts from Galapagos material and the overlying mantle wedge. The difference in Pb isotopic composition between the Pliocene-Quaternary central Costa Rica and the southern Costa Rica/western Panama lavas correlates closely with the boundary between the subducting Seamount province and Cocos/Coiba ridges of the chemically zoned Galapagos hotspot track. The subducting Seamount province and the Cocos/Coiba ridges, which have distinct Pb and Nd (Supplementary Fig. 1.1) isotopic compositions[18,19], could serve as the endmembers necessary for generating the distinct isotopic compositions of the central Costa Rica and southern Costa Rica/western Panama lavas, respectively. Fields for (1) fore-arc igneous terranes, which includes CLIP basement from Costa Rica and Panama[22,23,25] and (2) sediments and ocean crust subducting beneath Nicaragua[1,19] are also shown. All errors are reported as 2σ of the mean.

The along-arc variations in volcanic-front isotopic composition indicate that the Galapagos seamount component diminishes in quantity towards northwestern Nicaragua. These trends cannot be produced by upper plate variation. Although CLIP lithosphere underlies Costa Rica, its composition (included in the fore-arc igneous terranes field in Fig. 2c) is distinct from that of the Seamount province[22,23]. The volcanic-front isotopic trends also cannot be explained by systematic changes in the composition of the subducting plate. During ODP Leg 170, gabbro sills with OIB-type geochemical characteristics were drilled about 80 km north of the Seamount province[27], suggesting that the Galapagos hotspot may have affected a larger area than represented by the morphological expression of the hotspot track. However, it is unlikely that the plume spread out 500 km north of the Cocos ridge. When the hotspot track off Costa Rica formed, the CNS was located to the south of the hotspot[19], and plume material would have flowed south towards the ridge (not north). In addition, the gabbro sills from Leg 170 do not have Pb isotopic compositions that plot within the Seamount province, but rather compositions that plot within the Cocos/Coiba ridge field (Supplementary Information Section 1). Finally, a seamount on the Cocos plate subducting beneath central Nicaragua shows no evidence for the presence of Galapagos-type material in this area[19] but rather has the appropriate composition to serve as the depleted Nicaraguan endmember.

As the seamount component only appears to be present on the incoming plate off the Pacific coast of central Costa Rica, this signature must have been introduced into the wedge by a melt-like slab component from the subducting Seamount province and then transported northwest in the mantle wedge in melt pockets (possibly crystallized to form pyroxenite after leaving the slab and reacting with the overlying mantle wedge peridotite). Fluids from the subducting plate beneath Nicaragua flux the wedge, causing melting and mixing with the Galapagos seamount component. As the mantle is transported northwestwards, the seamount component will be progressively flushed out of the wedge, causing a decrease in Pb and increase in Nd isotopic composition.

Seismic anisotropy in the mantle wedge beneath Nicaragua and Costa Rica provides corroborating evidence for arc-parallel flow. Shear-wave splitting was measured in local S phases recorded by a dense temporary deployment of broadband seismometers (Supplementary Fig. 2.1), and a three-dimensional model of anisotropy was obtained (Fig. 3) by tomographically inverting the splitting measurements[28]. Beneath the arc where the Galapagos geochemical signature is observed and further into the back-arc, anisotropy is dominated by roughly arc-parallel alignment of the olivine fast symmetry axis (*a* axis). These *a* axes extend well into the warmer wedge where they should align roughly parallel to flow[6]. A zone of arc-normal *a* axes appears beneath the northwestern end of the Nicaraguan arc where geochemical evidence for the Galapagos seamount component is nearly absent, perhaps suggesting a reduction in arc-parallel flow.

The isotope data allow an along-arc flow rate for the mantle in the wedge to be directly estimated. Given that samples from the Miocene Nicaraguan arc (7–24 Myr old) adjacent to Quaternary southwest Nicaraguan rocks (Fig. 1) have Pb isotope ratios that overlap the range in the Quaternary northwest Nicaraguan volcanic front (Fig. 2), the component with elevated Pb isotope ratios was presumably introduced into the mantle beneath Nicaragua after the Miocene. Igneous rocks from the Miocene arc (6–26 Myr old) in Costa Rica have slightly more radiogenic isotopic compositions than those from Nicaragua, which could reflect interaction with CLIP lithosphere or derivation from subduction of older Galapagos hotspot tracks[24]. The Seamount province composition is not however observed in the Miocene volcanic rocks, providing a maximum age for the appearance of this component of ~6 Myr. Assuming that the oldest part of the subducted Seamount province lies along its boundary with the Panama fracture zone (Fig. 1), it would have passed beneath the central Costa Rican volcanic front 2–3 Myr ago[21] (reversing subduction at a rate of 85 mm yr^{-1}), providing a minimum age of 2 Myr for the appearance of the seamount component beneath the arc.

These dates (2–6 Myr ago) imply that the minimum arc-parallel wedge flow ranges from 63 to 190 mm yr^{-1}, assuming the Galapagos seamount component is transported a distance of 380 km. This distance is measured from the northwesternmost Nicaraguan volcano (Casitas) that shows a clear geochemical influence of the subducting

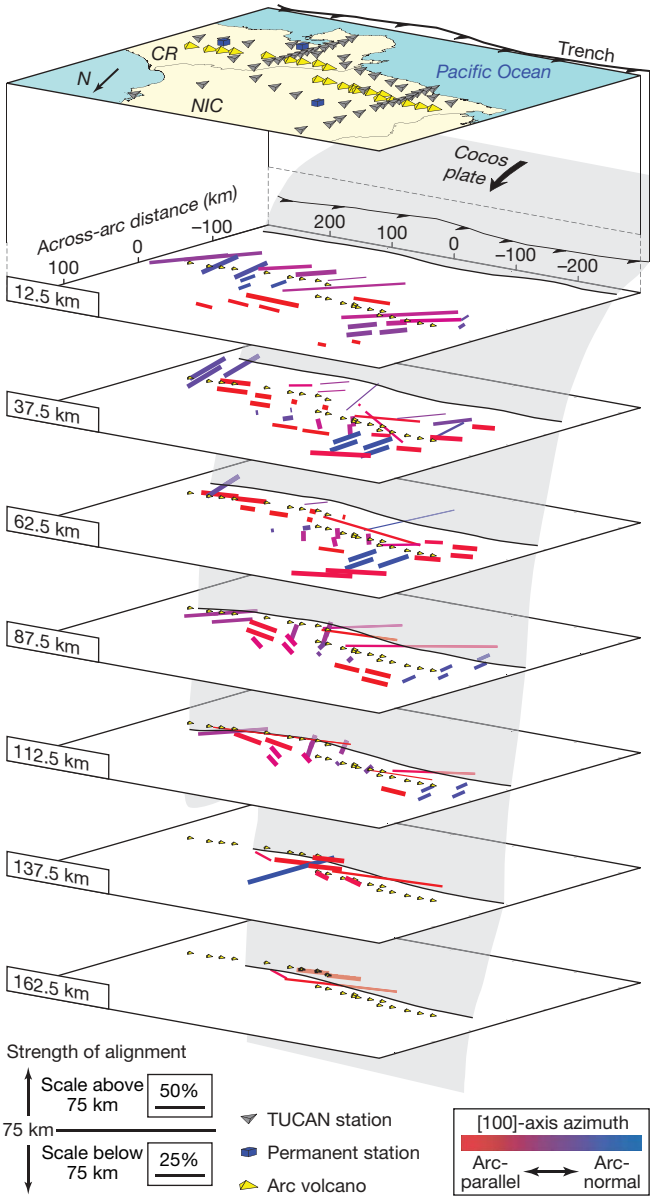

Figure 3 | Model of anisotropy obtained by inverting shear-wave splitting measurements from events in the Nicaragua (NIC)-Costa Rica (CR) subduction zone. The inversion used a tomographic approach[28] (see Methods and Supplementary Information Section 2). The vectors represent well-resolved olivine *a* axes in an olivine-orthopyroxene model, with orientation and colour indicating horizontal azimuth. Vector length corresponds to the strength of anisotropy relative to single-crystal values; note the change in strength scale at 75 km depth. We also invert for *a*-axis dip, but for clarity here we project *a* axes onto map-view planes. Effective block size in the rear- and back-arc is larger. Only well-resolved regions of the model are shown, and vector thickness corresponds to model parameter resolution. The TUCAN seismic array and volcanic arc are shown at the surface, and for reference, the volcanic arc is plotted on each slice through the model. The slab–wedge interface, based on earthquake locations, is shown by grey shading. The top two layers primarily lie within the upper plate; the mantle wedge is located in front of the slab in the layers spanning 50–175 km. Roughly arc-parallel *a* axes dominate well-resolved wedge regions beneath the arc and the rear- and back-arc at depths of 50–150 km, with the exception of a zone of arc-normal *a* axes at the northwestern end of the arc in Nicaragua and one isolated model block deep beneath the back-arc.

Seamount province (more radiogenic Pb and less radiogenic Nd than Cosigüina volcano and the crust subducting beneath Nicaragua) to the location of maximum Pb isotopic composition (greatest amount of Galapagos seamount component) in central Costa Rica. These transport rates are of the order of the Cocos plate subduction rate ($\sim$85 mm yr^{-1} off Costa Rica), suggesting that lateral (arc/trench-parallel) flow in the mantle wedge can compete with flow entrained by subduction.

Lead isotope data demonstrate that rapid arc-parallel flow occurs in the mantle wedge beneath Costa Rica and Nicaragua, allowing arc-parallel fast anisotropy to be explained without atypical mechanisms of generating anisotropic fabrics[5,14]. Trench rollback, variations in slab dip, and arc-parallel shearing within the upper plate may all contribute to along-arc wedge flow[9,13,16]. In Costa Rica and Nicaragua, the fore-arc is translating to the northwest, although at less than 15 mm yr^{-1} (ref. 29). Westward migration of the volcanic front since the early Miocene was greatest in Nicaragua and Honduras/El Salvador[30] (Fig. 1) where slab dips are steepest, suggesting differential slab roll-back that could draw wedge material towards northwestern Nicaragua, possibly from a slab window to the south. Collision (indenture) of the thickened Cocos ridge crust with the margin could also have helped drive arc material northwards. Regardless of the mechanism for generating flow, this study demonstrates a rate of arc-parallel flow beneath Costa Rica and Nicaragua that rivals downgoing Cocos plate motion.

METHODS SUMMARY

Nd and Pb isotope analyses were carried out at IFM-GEOMAR by thermal ionization mass spectrometry (TIMS), using a Triton and a MAT262 RPQ^{2+} TIMS, respectively. Over the course of the study, La Jolla produced ^{143}Nd/^{144}Nd = 0.511846 $\pm$ 0.000005 (N = 49) and the long-term reproducibility of NBS 981 (n = 184) is ^{206}Pb/^{204}Pb = 16.899 $\pm$ 0.007, ^{207}Pb/^{204}Pb = 15.437 $\pm$ 0.009, ^{208}Pb/^{204}Pb = 36.525 $\pm$ 0.028. Total chemistry blanks were $<$100 pg for Nd and Pb, and thus are considered negligible.

We solve for a best-fitting model of anisotropy through an iterative, damped, least-squares inversion[28] of 791 local-S splitting measurements from the TUCAN broadband seismic experiment. Anisotropy is described by a hexagonal average of olivine and orthopyroxene elastic coefficients, and parameters in each model block are the azimuth and plunge of the olivine *a* axis and a scalar that controls the strength of anisotropy. A total of 100 iterations were realized, with a moderate relaxation of damping after iteration 40. Model blocks are 25 km on each side, although in back-arc regions constraints were applied after iteration 70 that forced model parameters to be uniform across groups of blocks. Predicted splitting measurements and partial derivatives were calculated at every iteration for each hypocentre–station pair by progressively splitting an initially linearly polarized wavelet to account for the anisotropy encountered in each model block along the phase path.

Full Methods and any associated references are available in the online version of the paper at www.nature.com/nature.

Received 23 July; accepted 5 December 2007.
Published online 21 January 2008.

1. Feigenson, M. D., Carr, M. J., Maharaj, S. V., Juliano, S. & Bolge, L. L. Lead isotope composition of Central American volcanoes: Influence of the Galapagos plume. *Geochem. Geophys. Geosyst.* **5,** Q06001, doi:10.1029/2003GC000621 (2004).
2. Herrstrom, E. A., Reagan, M. K. & Morris, J. D. Variations in lava composition associated with flow of asthenosphere beneath southern Central America. *Geology* **23,** 617–620 (1995).
3. Abratis, M. & Wörner, G. Ridge collision, slab window formation, and the flux of Pacific asthenosphere into the Caribbean realm. *Geol. Soc. Am.* **29,** 127–130 (2001).
4. Goss, A. R. & Kay, S. M. Steep REE patterns and enriched Pb isotopes in southern Central American arc magmas: Evidence for forearc subduction erosion? *Geochem. Geophys. Geosyst.* **7,** Q05016, doi:10.1029/2005GC001163 (2006).
5. Jung, H. & Karato, S.-i. Water-induced fabric transition in olivine. *Science* **293,** 1460–1463 (2001).
6. Kneller, E. A., van Keken, P. E., Karato, S.-i. & Park, J. B-type olivine fabric in the mantle wedge: Insights from high-resolution non-Newtonian subduction zone models. *Earth Planet. Sci. Lett.* **237,** 781–797 (2005).
7. Nakajima, J., Shimizu, J., Hori, S. & Hasegawa, A. Shear-wave splitting beneath the southwestern Kurile arc and northeastern Japan arc: A new insight into mantle return flow. *Geophys. Res. Lett.* **33,** L05305, doi:10.1029/2005GL025053 (2006).
8. Long, M. D. & van der Hilst, R. D. Upper mantle anisotropy beneath Japan from shear wave splitting. *Phys. Earth Planet. Inter.* **151,** 206–222 (2006).
9. Smith, G. P. *et al.* A complex pattern of mantle flow in the Lau backarc. *Science* **292,** 713–716 (2001).
10. Levin, V., Droznin, D., Park, J. & Gordeev, E. Detailed mapping of seismic anisotropy with local shear waves in southeastern Kamchatka. *Geophys. J. Int.* **158,** 1009–1023 (2004).
11. Anderson, M. L., Zandt, G. & Wagner, L. Along-strike mantle flow variations in a segment of the South American subduction zone, Chile and Argentina. *Earth Planet. Sci. Lett.* (submitted).
12. Pozgay, S. H., Wiens, D. A., Conder, J. A., Shiobara, H. & Sugioka, H. Complex mantle flow in the Mariana subduction system: Evidence from shear wave splitting. *Geophys. J. Int.* **107,** 371–386 (2007).
13. Hall, C. E., Fischer, K. M. & Parmentier, E. M. The influence of plate motions on three dimensional back-arc mantle flow and shear wave splitting. *J. Geophys. Res.* **105,** 28009–28033 (2000).
14. Holtzman, B. K. *et al.* Melt segregation and strain partitioning: Implications for seismic anisotropy and mantle flow. *Science* **301,** 1227–1230 (2003).
15. Behn, M. D., Hirth, G. & Kelemen, P. B. Trench-parallel anisotropy produced by foundering of arc lower crust. *Science* **317,** 108–111 (2007).
16. Kneller, E. A. & van Keken, P. E. Trench-parallel flow and seismic anisotropy in the Mariana and Andean subduction systems. *Nature* **450,** 1222–1225 (2007).
17. Reagan, M. K. & Gill, J. B. Coexisting calcalkaline and high-niobium basalts from Turrialba volcano, Costa Rica: Implications for residual titanates in arc magma sources. *J. Geophys. Res.* **94,** 4619–4633 (1989).
18. Hoernle, K. A., Werner, R., Phipps Morgan, J., Bryce, J. & Mrazek, J. Existence of a complex spatial zonation in the Galápagos plume for at least 14.5 Ma. *Geology* **28,** 435–438 (2000).
19. Werner, R., Hoernle, K., Barckhausen, U. & Hauff, F. Geodynamic evolution of the Galapagos hot spot system (Central East Pacific) over the past 20 m.y.: Constraints from morphology, geochemistry, and magnetic anomalies. *Geochem. Geophys. Geosyst.* **4,** doi:10.1029/2003GC000576 (2003).
20. Defant, M. J. *et al.* The geology and geochemistry of El Valle volcano, Panama: Andesite and dacite genesis via contrasting processes. *Contrib. Mineral. Petrol.* **106,** 309–324 (1991).
21. MacMillan, I., Gans, P. B. & Alvarado, G. Middle Miocene to present plate tectonic history of southern Central American volcanic arc. *Tectonophysics* **392,** 325–348 (2004).
22. Hoernle, K., Hauff, F. & van den Bogaard, P. 70 m.y. history (139–69 Ma) for the Caribbean large igneous province. *Geology* **32,** 697–700 (2004).
23. Hauff, F., Hoernle, K. A., van den Bogaard, P., Alvarado, G. E. & Garbe-Schönberg, D. Age and geochemistry of basaltic complexes in Western Costa Rica: Contributions to the geotectonic evolution of Central America. *Geochem. Geophys. Geosyst.* **1,** doi:10.1029/1999GC000020 (2000).
24. Hoernle, K. A. *et al.* The missing history (16–71 Ma) of the Galápagos hotspot: Implications for the tectonic and biological evolution of the Americas. *Geology* **30,** 795–798 (2002).
25. Patino, L. C., Carr, M. J. & Feigenson, M. D. Local and regional variations in Central American arc lavas controlled by variations in subducted sediment input. *Contrib. Mineral. Petrol.* **138,** 265–283 (2000).
26. Carr, M. J., Feigenson, M. D. & Bennett, E. A. Incompatible element and isotopic evidence for tectonic control of source mixing and melt extraction along the Central American arc. *Contrib. Mineral. Petrol.* **105,** 369–380 (1990).
27. Kimura, G. *et al.* SITE 1039 (Ch. 3); SITE 1040 (Ch. 4). *Proc. ODP Init. Rep.* **170,** 45–152 (1997).
28. Abt, D. L. & Fischer, K. M. Resolving three-dimensional anisotropic structure with shear-wave splitting tomography. *Geophys. J. Int.* (submitted).
29. Turner, H. L. *et al.* Kinematics of the Nicaraguan forearc from GPS geodesy. *Geophys. Res. Lett.* **34,** L02302, doi:10.1029/2006GL027586 (2007).
30. Alvarado, G. E. *et al.* in *Central America: Geology, Resources and Hazards* (eds Bundschuh, J. & Avarado, G.) 345–394 (Taylor and Francis, Leiden, 2007).

Supplementary Information is linked to the online version of the paper at www.nature.com/nature.

Acknowledgements Reviewers (J. Walker and S. Schwartz), J. Phipps-Morgan, T. Plank, R. Werner, M. Portnyagin and members of SFB574 and MARGINS are thanked for comments/discussions that helped significantly improve the manuscript. The IRIS PASSCAL programme provided seismometers and technical assistance to the TUCAN experiment. This research was supported by the German Science Foundation Collaborative Research Centre (SFB574) and the National Science Foundation MARGINS programme.

Author Contributions K.H., D.L.A. and K.M.F. collected samples/data, processed and interpreted the data, developed the ideas and wrote the paper, with significant input from G.A.A. and discussions with other co-authors. H.N., F.H. and K.H. generated the geochemical data and P.v.d.B. age data. G.A.A., M.P. and W.S. were key in collecting the seismic data; P.v.d.B., G.A. and H.N. assisted in the collection of the volcanic samples. Central American partners provided geological overviews and logistical support.

Author Information Reprints and permissions information is available at www.nature.com/reprints. Correspondence and requests for materials should be addressed to K.H. (khoernle@ifm-geomar.de).

METHODS

Sample preparation and isotope analyses. Samples used in this study were cleaned of surficial dirt and then coarsely crushed into chips smaller than 4 cm. The chips were sieved and washed with deionized water, followed by ~12 h drying in a warm (50 °C) oven. Approximately 30–60 g of clean chips were hand-picked under a binocular microscope and ground to sand-sized particles in a mechanized agate mortar and pestle, followed by fine grinding in an agate mill by a shatter box. A subset of 0.5–1.0 mm sized chips was saved for Pb isotope analyses. Sample dissolution and element chromatography were carried out at the Leibniz Institute of Marine Sciences IFM-GEOMAR in Kiel (Germany) in Class 1000 clean rooms that are equipped with Class 100 laminar flow hoods. All reagents used were either double distilled in a PicoTrace Teflon distillery (HCl and HNO_3) or certified ultrapure HF and HBr acids from SEASTAR. An ELGA purifying system provided 18.2 MΩ water. Nd and Pb isotope analyses were carried out on whole rock powders (Nd) and rock chips (Pb) that were leached in hot 2 M HCl (70 °C, 1 h) in order to minimize the effects of alteration and sample handling. About 100 mg of sample was weighed into a Teflon beaker and then dissolved for 2 days in a 5:1 mixture of ultrapure HF and HNO_3 at 150 °C.

The ion chromatography followed established standard procedures[31]. These include a two-pass Pb separation and clean-up using 100 µl Teflon microcolumns filled with Bio-Rad AG 1X8 (100–200 mesh) resin that is equilibrated with 1 M HBr for highest Pb retention and from which Pb is released with 1 ml of 6 M HCl. The rare-earth elements (REEs) are obtained in 6 ml 6 M HCl at the final washout during Rb-Sr separation on quartz glass columns filled with Bio-Rad AG50W-X8 (100–200 mesh) resin. The REEs are then loaded in 0.25 M HCl onto 4 ml quartz glass columns filled with Eichrom Ln-Spec resin (100–150 µm) to obtain the Nd fraction. Pb and Nd isotopic ratios were determined by TIMS at IFM-GEOMAR on a MAT262 RPQ^{2+} and Triton TIMS, respectively. Both instruments operate in static multi-collection mode. Nd isotopic ratios are normalized within each run to $^{146}Nd/^{144}Nd = 0.7219$ and all errors are reported as 2σ of the mean. Over the course of the study, La Jolla produced $^{143}Nd/^{144}Nd = 0.511846 \pm 0.000005$ ($N = 49$) and our in-house Nd-monitor SPEX $^{143}Nd/^{144}Nd = 0.511711 \pm 0.000006$ ($N = 39$). Nd replicate analyses (separate digests) of 4 samples were within the external errors of the standards. The long-term reproducibility of NBS 981 ($N = 184$) is $^{206}Pb/^{204}Pb = 16.899 \pm 0.007$, $^{207}Pb/^{204}Pb = 15.437 \pm 0.009$, $^{208}Pb/^{204}Pb = 36.525 \pm 0.028$. Pb isotope ratios are normalized to published NBS 981 values[32]. Pb replicate analyses (separate digests) of 13 samples were on the average better than 0.022% per AMU. Total chemistry blanks were <100 pg for Nd and Pb and thus are considered negligible.

Shear-wave splitting analysis and tomography method. We analysed shear-wave splitting in local S phases recorded by the TUCAN broadband seismic experiment and by three permanent stations, maintained by the GSN (IRIS), GEOSCOPE (France) and GEOFON (Germany). Over the 20-month deployment, we obtained 791 high-quality splitting measurements (Supplementary Fig. 2.1) using an eigenvalue minimization method[33]. We inverted these local S splitting measurements for a three-dimensional model of anisotropy (Fig. 3 and Supplementary Fig. 2.3).

Here we briefly highlight the key aspects of this technique; the method is described in detail elsewhere[29]. The elastic coefficients of the anisotropic model were assumed to be an average of olivine and orthopyroxene[34–36]. The model was divided into blocks (25 km per side), and parameters in each block are the azimuth and plunge of the olivine *a* axis and a scalar value that controls the strength of anisotropy relative to its single-crystal value. The model in Fig. 3 and Supplementary Fig. 2.3 assumes hexagonal symmetry for the anisotropy, but inversions assuming orthorhombic symmetry yield similar results.

The inversion was conducted using an iterative, damped least-squares approach. The starting model was constructed by prescribing the average fast direction for all phases that sample a block as the olivine *a* axis azimuth in that block. The fabric strength in the starting model was based on the average splitting times from each ray within a block relative to that predicted from the single-crystal elastic coefficients. Synthetic splitting was calculated by propagating, for each ray, an initially linearly polarized wavelet through successive anisotropic blocks along its path and accruing splitting from each block until the phase reached the station[37]. Shear-wave splitting parameters were determined from the resulting waveform using the same method applied to the data[33] and then were used to calculate data–model residuals and partial derivatives.

Inversions were performed using a wide variety of starting models, block sizes and damping parameters. Even when optimal inversion parameters were used, some model blocks in the back-arc remained poorly resolved because of reduced ray coverage. Therefore, effective block size was made larger in back-arc regions to permit interpretation of a larger portion of the model space, albeit at coarser spatial resolution. The size of these larger (non-cubic) model volumes is variable, but is typically 50 km thick and between 50 km and 100 km in each horizontal direction (Supplementary Fig. 2.4).

To test the accuracy with which the *a* axis orientation and fabric strength can be retrieved, inversions of synthetic data predicted by a series of anisotropic target models were carried out using the source–station distribution for the TUCAN shear-wave splitting data set[28]. For target models that vary laterally in better sampled model regions (beneath the fore-arc, arc, and regions of the back-arc near the dense arc-normal lines of stations) with uniform anisotropy elsewhere, *a* axis orientation is retrieved to within 25° on average; *a* axis azimuth is, in general, recovered at high accuracy down to at least 100 km depth, and *a* axis dip recovery is typically good to roughly 75 km. Lateral variations at spatial scales of 50–75 km can be imaged beneath the arc, but retrievable spatial variations are obviously coarser in back-arc regions where individual blocks are grouped into larger volumes (Supplementary Fig. 2.4).

31. Hoernle, K. A. & Tilton, G. R. Sr-Nd-Pb isotope data for Fuerteventura (Canary Islands) basal complex and subaerial volcanics: Applications to magma genesis and evolution. *Schweiz. Mineral. Petrogr. Mitt.* **71,** 3–18 (1991).
32. Todt, W., Cliff, R. A., Hanser, A. & Hofmann, A. W. in *Earth Processes: Reading the Isotopic Code* (eds Basu, A. & Hart, S.) 429–437 (AGU Geophys. Monogr. Ser. 95, American Geophysical Union, Washington DC, 1996).
33. Silver, P. G. & Chan, W. W. Shear wave splitting and subcontinental mantle deformation. *J. Geophys. Res.* **96,** 16429–16454 (1991).
34. Frisillo, A. L. & Barsch, G. R. Measurement of single-crystal elastic constants of bronzite as a function of pressure and temperature. *J. Geophys. Res.* **77,** 6360–6384 (1972).
35. Anderson, O. L. & Isaak, D. G. in *Mineral Physics and Crystallography: A Handbook of Physical Constants* (ed. Ahrens, T. J.) 64–97 (American Geophysical Union, Washington DC, 1995).
36. Abramson, E. H., Brown, J. M., Slutsky, L. J. & Zaug, J. The elastic constants of San Carlos olivine to 17 GPa. *J. Geophys. Res.* **102,** 12253–12263 (1997).
37. Fischer, K. M., Parmentier, E. M., Stein, A. R. & Wolf, E. R. Modeling anisotropy and plate-driven flow in the Tonga subduction zone back arc. *J. Geophys. Res.* **105,** 16181–16191 (2000).